Unsteady Flow Around an Ogive Cylinder

Mohamed Gad-el-Hak* and Chih-Ming Ho†
Flow Research Company, Kent, Washington

The time-dependent flow around an ogive cylinder undergoing large-amplitude, harmonic pitching motion was investigated using flow visualization techniques. The slender body of revolution was towed in an 18 m water channel at Reynolds numbers up to 1.2×10^5. Fluorescent dyes were either introduced uniformly from the body's porous surface or placed as horizontal sheets in the slightly stratified tank prior to a run. The dyes were excited with a sheet of laser light projected in the desired plane to mark the flow in the separation region around the body, the flow in the wake, and the potential flow away from the body. The separation process and the geometry of the leeward vortices were studied under different reduced frequencies and Reynolds numbers. The unsteady separation phenomenon is found to be significantly different from the separation on a body in steady flight. Two distinct separation regions, the forebody and aftbody vortex pairs, evolve in the unsteady case.

Nomenclature

D = maximum body diameter
f = pitching frequency
H = height of separation region
K = reduced frequency, $\pi fD/U_\infty$
L = body length
R_D = Reynolds number, $U_\infty D/\nu$
t = time, s
U_∞ = towing speed
x,y,z = Cartesian coordinates fixed with the body
$\alpha(t)$ = time-dependent angle between the body centerline and the towing direction
$\dot{\alpha}(t)$ = rate of change of angle of attack
$\alpha_A(t)$ = time-dependent angle between the body centerline and the relative velocity vector (aerodynamic angle of attack)
α_0 = mean pitching angle
α_{00} = amplitude of harmonic motion
β = angle between the plane of symmetry of the separation vortex and the vertical axis
ν = kinematic viscosity

I. Introduction

THERE has been recent interest in the concept of supermaneuverability where previously unattained regions of the maneuver envelope for a fighter aircraft are attempted, such as poststall flight maneuvers and side slipping.[1,2] The performance of a highly maneuverable aircraft is critically dependent upon the accurate prediction of the flow around the wings, body, and other parts of the vehicle. While the wings are of the utmost importance aerodynamically, the unsteady flow around the body must play a role in the maneuverability of the airplane. Similarly, an understanding of the unsteady flow around a missile is essential for predicting the aerodynamic forces during maneuvering. These forces are not constrained by pilot limitations and a missile can therefore operate at higher normal accelerations and higher angles of attack (beyond the linear range) than a typical aircraft.

Received Oct. 29, 1985; presented as Paper 86-0572 at the AIAA 24th Aerospace Sciences Meeting, Reno, NV, Jan. 6-9, 1986; revision received March 10, 1986.

*Senior Research Scientist. Member AIAA.
†Scientist; presently Professor, Department of Aerospace Engineering, University of Southern California, Los Angeles. Member AIAA.

At high angles of attack, the symmetric leeward separation on an axisymmetric body is exceedingly complex; thus, progress in forming the basis for describing and modeling how vorticity is shed from the body to the leeward wake has depended crucially upon experiment.[3] While much remains to be investigated, a reasonable overall understanding of the steady flow around an axisymmetric body is evolving. Unfortunately, little is known about the influence of time-dependent motions (e.g., pitching oscillations) on the time evolution of the leeward vortex structure or the flowfield in general. In his broad survey of missile aerodynamics, Nielsen[3] does not even discuss time-dependent motions. This is unlike the relatively large body of past and ongoing theoretical and experimental research dealing with unsteady flows around two- and three-dimensional airfoils.[4-20]

Motivated by the need to design rapidly maneuvering torpedoes and submarines, some of the early work considered the hydrodynamic forces acting on a body of revolution undergoing a periodic change of incidence. Szebehely and Niederer[21] were perhaps the first to conduct an experiment to find the effects of frequency and amplitude of oscillations on the forces acting on a prolate spheroid, which had a 7:1 fineness ratio and was oscillated in yaw about a vertical axis. Another important contribution was made by Sevik,[22] who oscillated an ellipsoid of revolution at a constant amplitude in a direction normal to the oncoming stream and measured the instantaneous pressure at various points on the body.

Extreme flight agility requirements for tactical missiles stimulated more research. References 23 and 24 established baseline static areodynamic data for a right circular cylinder with a three-caliber tangent-ogive nose and an overall length-to-diameter ratio of 15:1. The static data were used to illustrate the influence of a constant rate of pitch upon the aerodynamic loads for large excursions in the angle of attack. Ericsson and Reding[25,26] discussed at length the dynamics of forebody flow separation and the unsteady, vortex-induced, asymmetric loads on slender vehicles. In Ref. 26, they analyzed the strong coupling between the body motion and the separation vortices and showed how the "moving-wall" effects can explain some anomalous results obtained in previous dynamic tests. An engineering rational flow model to predict the aerodynamic characteristics and motion of a missile in unsteady maneuvers was developed in Ref. 27.

While these studies provide extremely useful information on the gross aerodynamic properties of the flowfield, much of the physics is still lacking. This is due in part to the scarcity of visualization results concerning the unsteady separa-

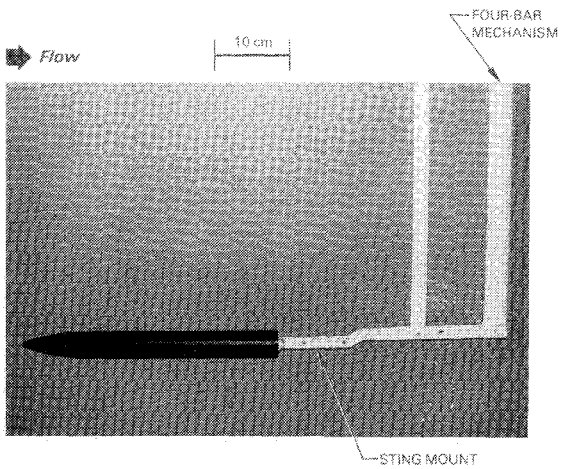

Fig. 1 Slender body and support system.

tion region. To provide a closer look at the unsteady motion around a body of revolution, flow visualization techniques were used in the present investigation to study the time-dependent flow around an ogive cylinder undergoing large-amplitude, harmonic pitching motion. The slender body was towed in an 18 m water channel and the flow was visualized using fluorescent dyes and sheets of laser light. The apparatus and the visualization method are described in the next section. In Sec. III, the unsteady separation phenomenon is described and the effects of changing the Reynolds number and the reduced frequency are categorized and elaborated. Conclusions are presented in Sec. IV.

II. Experimental Approach

The flow over an ogive cylinder undergoing a time-dependent pitching motion about $x/L=0.5$ was studied. The slender body of revolution is made of polyvinyl chloride plastic. The pointed ogive nose has a fineness ratio of 3, a radius of curvature at the tip of 0.45 cm, and a maximum diameter of 4 cm. The overall fineness ratio of the body is 10. The body was towed in the water channel described in Ref. 28. This towing tank is 18 m long, 1.2 m wide, and 0.9 m deep and the towing speed U_∞ was varied in the range of 5-300 cm/s. This provided a Reynolds number range of $2\times10^3 \le R_D \equiv U_\infty D/\nu \le 1.2\times10^5$, where D is the maximum body diameter and ν the kinematic viscosity.

A four-bar mechanism was used to sting mount (Fig. 1) and pitch the body around the desired position along its length. In the experiments reported here, the body was pitched around $x=0.5\ L$, where x is the distance along the axis of symmetry measured from the nose and L the body's length. The mean angle of attack could be set at 0-45 deg, but was set at 15 deg for this investigation. A Boston Ratiotrol motor drove the four-bar linkages to produce approximately sinusoidal oscillations at amplitudes of ±5, ±10, or ±15 deg about a given mean angle of attack and at frequencies up to 1 Hz. The reduced frequency, $K\equiv\pi fD/U_\infty$, where f is the pitching frequency, was varied in the range of 0.04-0.75. A digital readout displayed the instantaneous angle between the body centerline and the towing direction $\alpha(t)$.

The complex, unsteady, separated flow around the slender body was visualized using a previously developed dye layer technique.[29] Horizontal layers of fluorescent dye were placed in a weakly stratified water channel prior to towing the body and excited using sheets of laser light projected in the desired plane. Longitudinal and transverse planes of the flowfield were visualized to provide better detail and to locate precisely the separation vortex position. The dye layers marked the flow in the separation region around the body, the flow in the wake region, and the potential flow away from the lifting surface. For more detailed visualization of the separation vortices, fluorescent dye was continuously seeped into the flow from the entire body surface. This was accomplished by covering the body with a thin, porous cloth saturated with (dry) dye crystals. As the body moved through the tank, the dye dissolved slowly into the surrounding water and marked the leeward vortices rather well. The visualization results were recorded using 35 mm photographs and 16 mm ciné films.

III. Results and Discussion

For a particular run, a few selected side and end views of the flow will be depicted here as still photographs. However, a visual image of the complex flowfield can be more readily constructed by viewing the ciné films (available from the first author upon request) in as many longitudinal and transverse planes as possible. As the first (starting) oscillation cycle is different from the second or subsequent cycles, it will not be shown in any of the figures presented here.

Forebody and Aftbody Vortices

The separation pattern for a pitching slender body is quite different from that for a body in steady flight. At a constant angle of attack, the boundary-layer fluid separates along lines on the lee side due to the forward motion of the body.[30] Discrete vortices[31] are formed by the rolling up of the resulting sheets of vorticity. These vortices are symmetrical at angles of attack less than approximately 20 deg (depending on the cross-flow Reynolds number), becoming asymmetric at moderate-to-large attack angles.[32-34] The asymmetric vortices are shed at first in a spatially periodic pattern, becoming unsteady at higher angles of attack.

For a pitching missile, separation may also be triggered by the harmonic motion. The reduced frequency, $K\equiv\pi fD/U_\infty$, determines the relative importance of the harmonic and forward motions. Let the angle between the missile axis and the towing direction be expressed as

$$\alpha(t)=\alpha_0+\alpha_{00}\sin(2\pi ft)$$

where α_0 and α_{00} are the mean pitching angle and amplitude of the harmonic motion, respectively, f the pitching frequency, and t the time. It can be shown by considering the relative velocity vector and after some algebra that the aerodynamic angle of attack (i.e., the angle between the missile axis and the relative velocity vector) at the the nose α_A is as follows for rotation around $x/L=0.5$:

$$\alpha_A(t)=\alpha(t)-\arctan\left[\frac{\pm\pi fL\phi(t)\cos\alpha}{U_\infty\mp\pi fL\phi(t)\sin\alpha}\right]$$

where $\phi(t)\equiv\sqrt{2\alpha\alpha_0-\alpha^2+\alpha_{00}^2-\alpha_0^2}$ and the sign change reflects whether α is increasing (upstroke) or decreasing (downstroke). As an example, for $f=0.16$ Hz and $U_\infty=10$ cm/s ($K=0.2$), the above equation for the aerodynamic angle of attack at the nose yields a value of $\alpha_A=-6$ deg when $\alpha=5$ deg and is increasing and a value of $\alpha_A=32$ deg for $\alpha=20$ deg during the downstroke. This effect is more pronounced for a larger pitching frequency or smaller towing speed. Similar expressions could easily be derived for other positions along the body, where the relative velocity vector is different for each location.[35,36] Of course, $\alpha_A(t)=\alpha(t)$ at the pivot point, $x/L=0.5$.

The above effects are best illustrated using side views of the flowfield. Figure 2 shows horizontal dye layers excited by a vertical sheet of laser light parallel to the towing direction and at $z/D=0.25$ off the body centerline. In the photographs, the laser sheet is projected from top to bottom and, hence, the model's shadow appears as a dark region. The flow is from left to right and the slender body underwent the pitching motion $\alpha(t)$ deg $=15+15\sin(2\pi ft)$, where

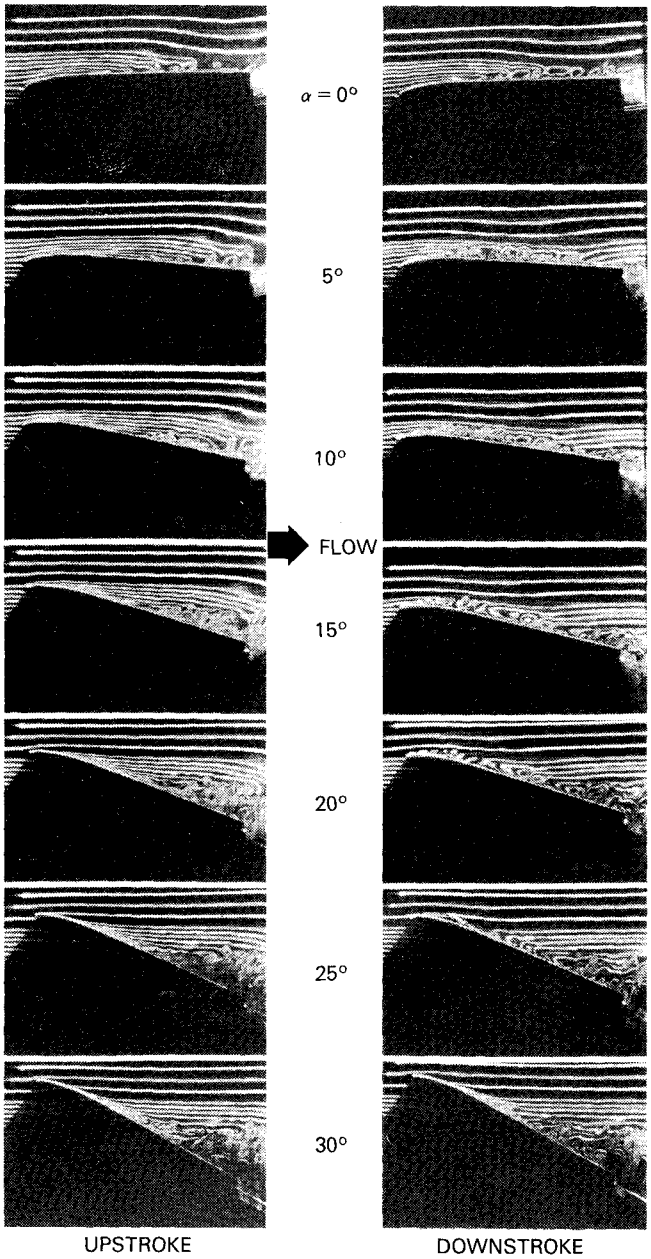

Fig. 2 Side view of the slender body undergoing a pitching motion: $R_D = 4\times10^3$, $K = 0.2$, $\alpha(t)^\circ = 15 + 15^\circ \sin(t)$ (vertical sheet of laser is parallel to the flow at $z = 1.0$ cm).

$2\pi f = 1$ rad/s. The Reynolds number based on the body's diameter was $R_D \equiv U_\infty D/\nu = 4\times10^3$ and the reduced frequency was $K \equiv \pi f D/U_\infty = 0.2$. The photographs show a typical oscillation cycle for both the upward and downward motions of the body at $\alpha = 0$, 5, 10, 15, 20, 25, and 30 deg. It is clear that two distinct separation regions evolve in the unsteady case. We term these the "forebody and aftbody separations." The former occurs mainly in the nose region during the downstroke and the latter evolves during the upstroke and starts near the tail of the body. The aftbody separation is farthest aft at about $\alpha = 5$ deg during the upstroke (the model's base is moving downward). The pitching motion causes a high-velocity graident to exist, creating a shear layer on either side of the body. The unstable shear layers roll up into a pair of counter-rotating vortices and the light sheet intersects one of the two structures. The aft separation propagates upstream at a speed of about 0.2 U_∞ and then slows down to a very low speed (0.05 U_∞) in the second half of the upstroke, reaching $x = 0.4\ L$ at the maximum angle of attack $\alpha = 30$ deg. At the beginning of

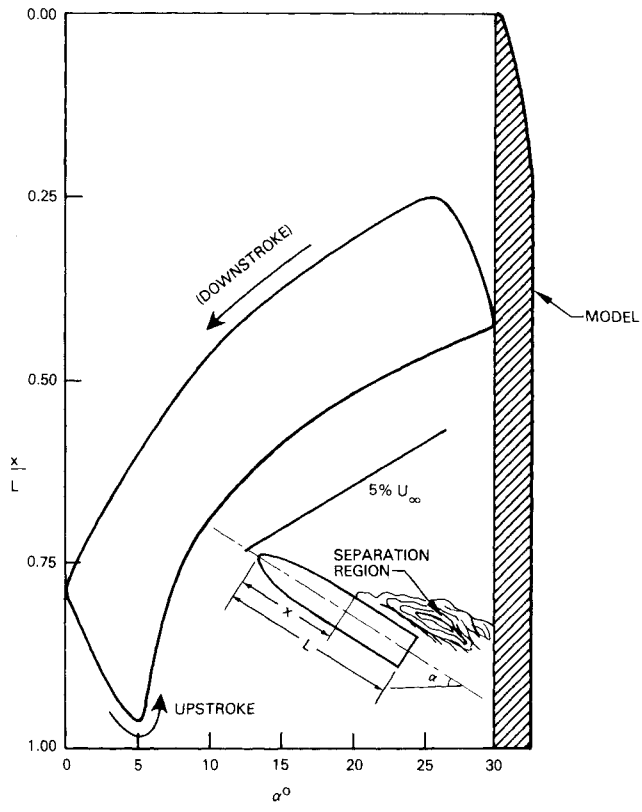

Fig. 3 Foreward propagation of the aft separation ($R_D = 4\times10^3$, $K = 0.2$).

the downstroke, a thin layer of fluid keeps propagating upstream. At $\alpha = 25$ deg, the reverse flow reaches the nose region of the body. The resulting intense shear, produced by the thin reverse flow region, seems to trigger the formation of a second pair of counterrotating vortices. These vortices, termed forebody separation, continue to grow as the angle of attack decreases to 10 deg, but decay for the rest of the downstroke.‡ The primary separation starts moving downstream as the incidence angle decreases, initially at a speed of about 0.05 U_∞, increasing to about 0.15 U_∞ at $\alpha = 10$ deg. Similar unsteady separation processes have been observed for two-dimensional airfoils undergoing large-amplitude pitching motion, where a primary trailing-edge separation seems to trigger a secondary leading-edge separation.[37-39]

The moving-wall effects discussed in Refs. 25 and 26 are expected to be large in the present experiments because of the relatively high values of reduced frequencies used and, hence, the strong axial variations (including a sign change at the rotation center) in the local aerodynamic angle of attack $\alpha_A(x,t)$. The local cross-flow separation is directly influenced by these effects, which may account for the presence of separate forebody and aftbody symmetric vortices.

As will become more apparent later in this paper when the end views are presented, the large separation region shown in Fig. 2 near the tail of the body at $\alpha > 15$ deg represents the cumulative signature of several different flow phenomena on the dye marker. These are 1) the aftbody vortex, originating in that region; 2) the forebody vortex, starting at the nose and convecting downstream; and 3) the turning of the forebody vortex into the longitudinal plane of the photographs. The signature of the foreward and aftbody vortices can be distinguished by viewing the first and second oscillation

‡This is true only in the vicinity of the nose. As will be seen later in the paper, the forebody separation propagates downstream; and, near the body's base, the vortex reaches its maximum height at $\alpha = 10$ deg during the *upstroke*.

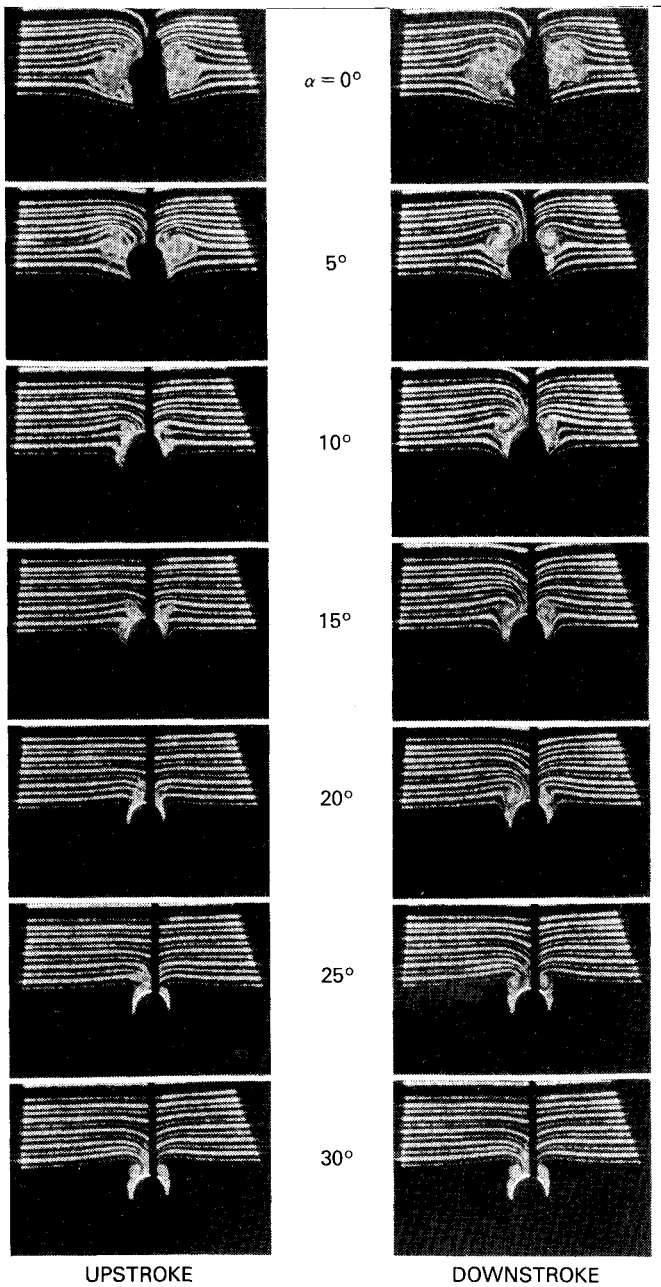

Fig. 4 End view using the dye-layer technique: $R_D = 4 \times 10^3$, $K = 0.2$; $\alpha(t)^\circ = 15 + 15^\circ \sin(t)$ (vertical sheet of laser at $x/L = 0.75$).

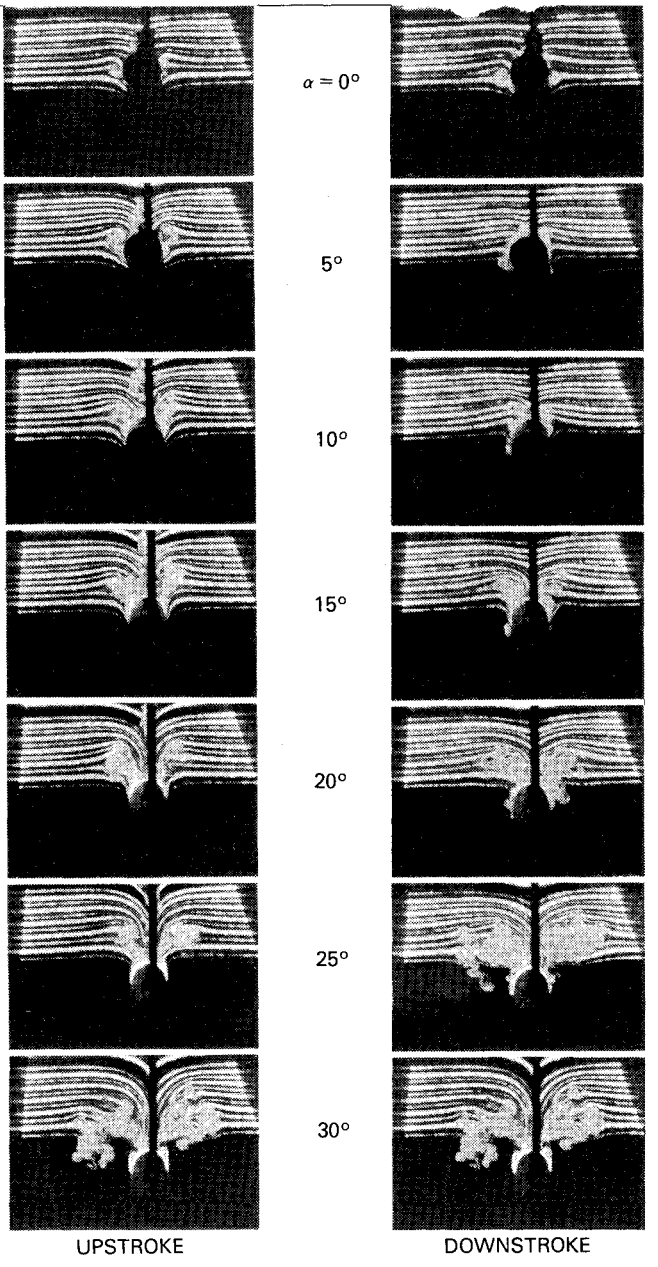

Fig. 5 End view using the dye-layer technique: $R_D = 4 \times 10^3$, $K = 0.4$; $\alpha(t)^\circ = 15 + 15^\circ \sin(2t)$ (vertical sheet of laser at $x/L = 0.75$).

cycles. During the first upstroke, the forebody vortices are not as yet formed and only the rear vortex pair is observed. Some information regarding the geometry of the two vortex pairs can then be obtained from the visualization results. Near the body's base and at the reduced frequency of $K = 0.2$, the aft separation vortices achieve their maximum height at $\alpha = 20$ deg during the downstroke, while the forebody vortex pair is largest at $\alpha = 10$ deg during the upstroke motion. In the streamwise direction, the heights of both the foreward and aft vortices grow almost linearly with distance along the body, indicating a nearly conical shape of the two vortex pairs at each phase of the pitching motion.

The position of the separation can be readily measured from the ciné films at each phase of the cycle. A typical example is shown in Fig. 3 for the aftbody separation occurring on the pitching missile at the run conditions depicted in Fig. 2. The distance x from the nose is nondimensionalized using the body length L. Note that in Fig. 3 the ordinate represents a missile pointing upward with its base at $x/L = 1.0$ (one-half of the model is sketched on the right-hand side of the figure).

Effects of Reduced Frequency

There are at least three time scales in the unsteady flow generated by a pitching body: the period of the oscillating motion, the time for the aftbody separation to propagate from the tail toward the nose of the body, and the time required for upstream crossflow effects to propagate downstream. The base flow phenomenon for slender bodies with bulbous bases[40,41] illustrates the competition between the cross-flow effects propagated downstream and the base flow effects propagated upstream. The dimensionless frequency K is the ratio of a pitching velocity scale to the flow speed or, alternatively, the ratio of a convection time scale to a pitching period. At low reduced frequencies, the separation vortices convect at a faster rate relative to an oscillation period and the flow has more time to adjust to angle-of-attack variations. Conversely, when the reduced frequency is large, the period of oscillation is short and the vortices have less time to adjust. Two reduced frequencies, $K = 0.2$ and 0.4, are depicted in the end views in Fig. 4 and 5. An underwater movie camera was towed behind the body and, hence, the ambient flow is out of the plane of the photographs in both figures. The dye layers were excited with a vertical sheet

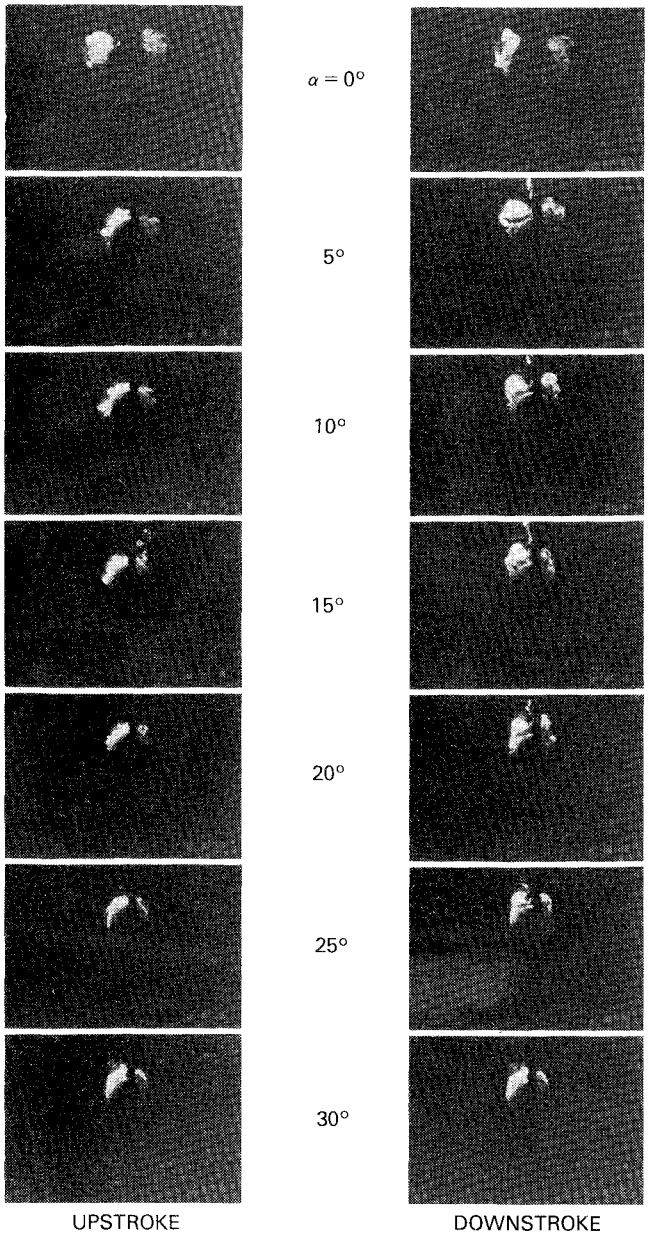

Fig. 6 End view of the slender body undergoing a pitching motion: $R_D = 4 \times 10^3$, $K = 0.2$ (vertical sheet of laser at $x/L = 0.5$).

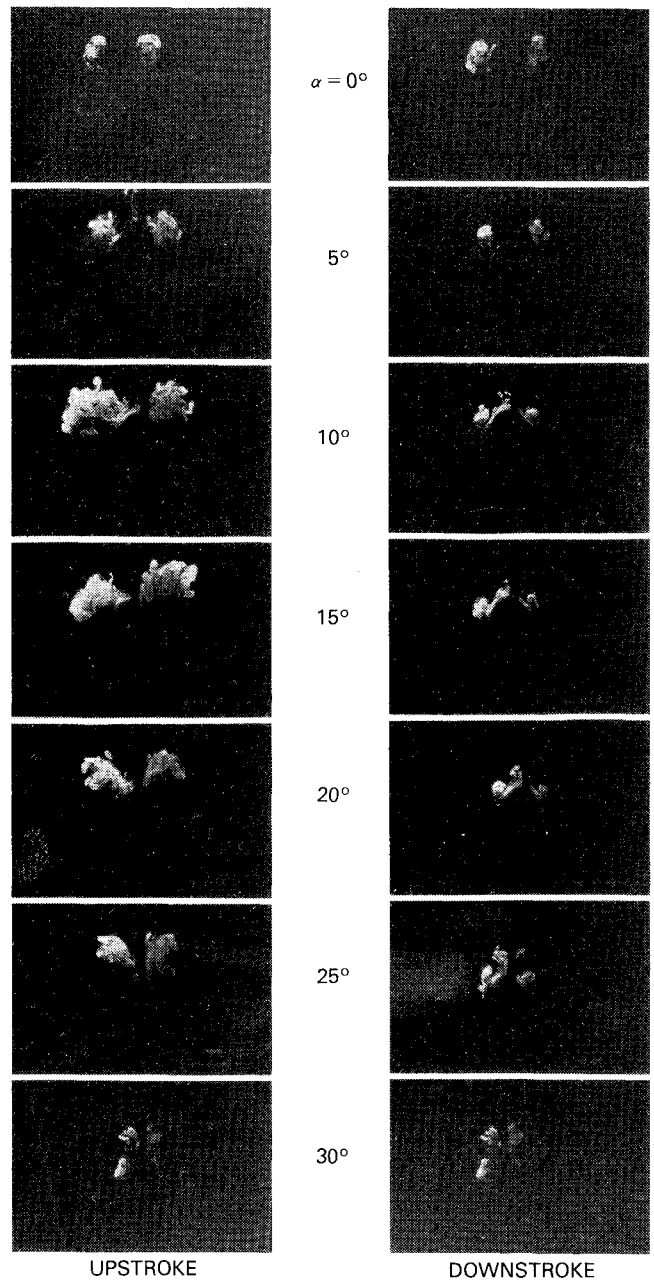

Fig. 7 End view of the slender body undergoing a pitching motion: $R_D = 4 \times 10^3$, $K = 0.2$ (vertical sheet of laser at $x/L = 0.75$).

of laser light perpendicular to the towing direction at $x/L = 0.75$.§ Again, the body's shadow caused by the projection of the laser sheet from top to bottom is seen in the photographs as darkened regions. For both runs, the body underwent the pitching motion $\alpha(t)\text{deg} = 15 \pm 15$ deg the Reynolds number was $R_D = 4 \times 10^3$. At the lower reduced frequency, $K = 0.2$, the forebody vortices from one cycle convect to this position ($x/L = 0.75$), at the beginning of the following cycle ($\alpha = 0$ deg). On the other hand, for the higher reduced frequency ($K = 0.4$), the arrival time is delayed to the end of the upstroke of the following cycle ($\alpha = 30$ deg). The photographs show clearly the evolution of the aftbody vortices and their interaction with the forebody vortices. Strong downward motion in the dye layers above the body, induced by the vortices, is more readily observed at the higher reduced frequency (Fig. 5). Note that temporal changes in the dye pattern in the plane of visualization result from fluid particles moving in this plane as well as from particles that are crossing the sheet of laser light.

§This is the position of the light sheet when the body is at zero angle of attack. As the missile pitches, the vertical sheet of laser intersects positions along the body progressively toward its tail. For example, at $\alpha = 30$ deg, the light sheet marks the station $x/L = 0.79$, as compared to $x/L = 0.75$ at $\alpha = 0$ deg.

Streamwise Evolution of the Separation Vortices

Both the foreward and aft vortex pairs undergo a growth/decay cycle as the angle of attack changes, much the same as the growth/decay cycle observed for the leading-edge vortices on a pitching delta wing.[19,20] End views using transverse sheets of light at different streamwise positions were used in the present experiments to study the evolution of the separation vortices. The laser light excited the fluorescent dye that was seeped continuously from the porous body surface. Three such views are presented in Figs. 6-8, for $x/L = 0.5$, 0.75, and 1.0, respectively. In all three runs, the Reynolds number was $R_D = 4 \times 10^3$, with the missile undergoing the harmonic pitching motion $\alpha(t)\text{deg} = 15 + 15$ deg $\sin(2\pi ft)$ at the reduced frequency $K = 0.2$ ($2\pi f = 1$ rad/s). It is interesting to compare Figs. 4 and 7, which represent identical run conditions but different visualization methods. The dye

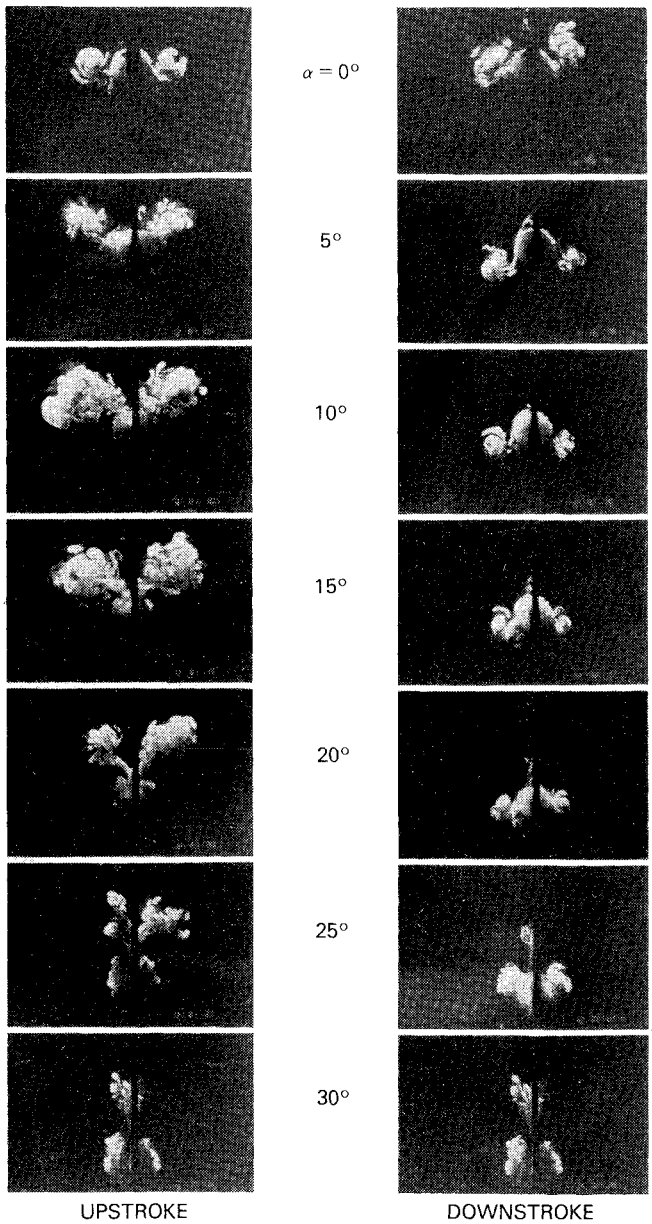

Fig. 8 End view of the slender body undergoing a pitching motion: $R_D = 4 \times 10^3$, $K = 0.2$ (vertical sheet of laser at $x/L = 1.0$).

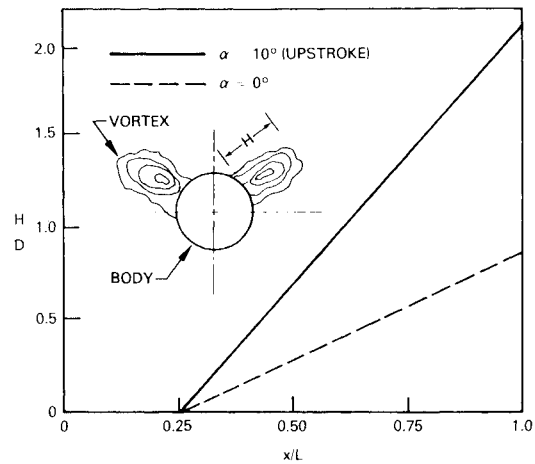

Fig. 9 Streamwise growth of the forebody vortices: $R_D = 4 \times 10^3$, $K = 0.2$.

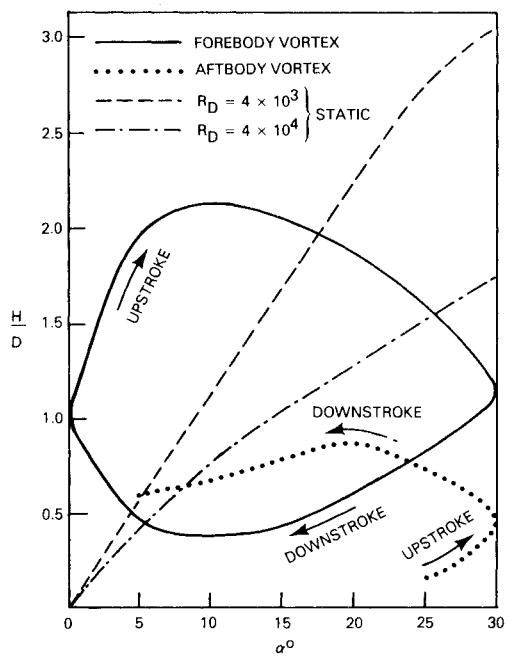

Fig. 10 Evolution of forebody and aftbody vortices: $R_D = 4 \times 10^3$, $K = 0.2$, $x/L = 1.0$.

layers placed in the tank prior to towing the model mark the flow (Fig. 4) quite differently from the dye seeping continuously from the body surface (Fig. 7). This is due to the well-known fact that flow visualization with dye depicts the integrated history of the marker's motion rather than its local (instantaneous) behavior.[42] Consequently, the observed results are a strong function of the method of introducing the dye into the flowfield.

The mutual induction between the vortices produces a strong downward motion of the vortex pair. As shown in Fig. 8 for $x/L = 1.0$, the aft vortices do not follow the motion of the body. During one pitching cycle, the base of the missile moves downward and then upward as the angle of attack changes from 0 to 30 and back to 0 deg. The aft vortices continue to move downward relative to the body, however, and are actually below the aftbody at $\alpha = 5$ deg during the downstroke.

From the end views, the size variation of the two vortex pairs during an oscillation period can be determined. The vortices clearly undergo a hysteresis loop. For example, at $x/L = 1.0$ (Fig. 8), the forebody vortex pair has a maximum height at $\alpha = 10$ deg during the upstroke, while the aftbody vortices reach a maximum height at $\alpha = 20$ deg during the downstroke. It also appears from the transverse cuts of the separation regions that both the forebody and aftbody vortex pairs are symmetric.

Geometry of the Vortex Pairs

The streamwise growth of the forebody vortices is obtained from the transverse views at different streamwise locations. The results for a reduced frequency of $K = 0.2$ and Reynolds number of $R_D = 4 \times 10^3$ are shown in Fig. 9, where H is the vortex height as sketched in the insert in the figure.¶ The broken line represents data for $\alpha = 0$ deg, while the solid line maps the vortex growth at $\alpha = 10$ deg during the upstroke. The linear behavior is striking and may indicate that such vortex pairs are amenable to theoretical modeling.

At any particular angle of attack, the flow patterns were very different during the upward and downward motions, indicating the existence of a hysteresis loop. The hysteresis in the vortex pair growth is seen in Fig. 10, which depicts the variation of the separation region height H as the angle of

¶This height is an indication of only the extent of the vortical region. In an unsteady flow, there is no precise relationship between H and the cross-flow streamlines or vorticity.

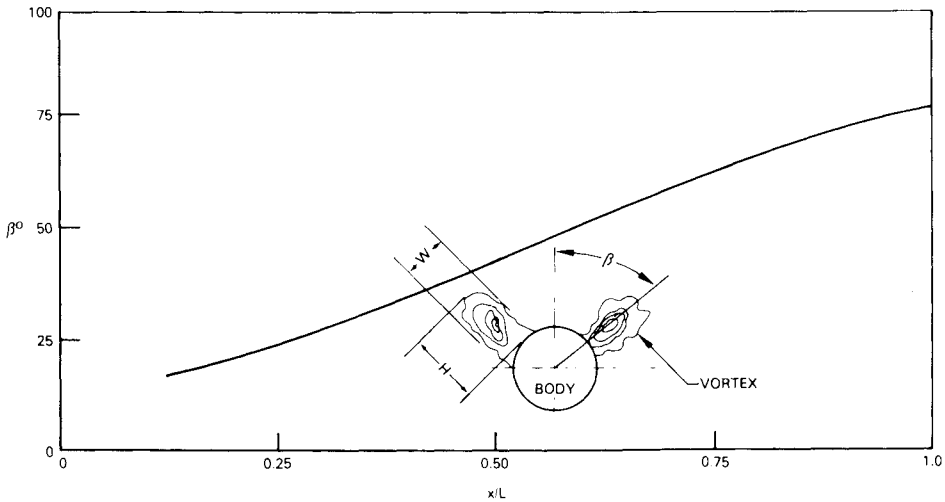

Fig. 11 Streamwise variation of β: $R_D = 4 \times 10^3$, $K = 0.2$; $\alpha = 15$ deg (upstroke).

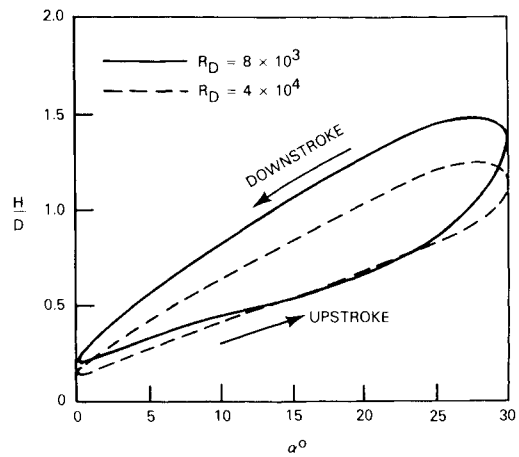

Fig. 12 Effects of Reynolds number on the hysteresis loop: $K = 0.04$, $x/L = 0.75$.

attack changes. The evolution for both the forebody and aftbody vortex pairs at $x/L = 1.0$, $K = 0.2$, and $R_D = 4 \times 10^3$ is shown in the figure. For reference, the height of the steady-state vortex pair is also plotted for two Reynolds numbers, $R_D = 4 \times 10^3$ and 4×10^4. At the same Reynolds number, the separation region at $\alpha = 30$ deg is about three times larger in the steady case than that for the pitching body.

An interesting quantity that further characterizes the separation vortices is the angle β between the plane of symmetry of the vortices and the vertical axis, which indicates the relative location of the vortices along the side of the body. This angle changes as the angle of attack varies and increases along the body length. Near the nose of the missile, the forebody vortices are located near the top (small β). At positions further downstream, the vortices gradually shift toward the sides of the body and β increases. As seen in Figs. 7 and 8 for $x/L = 0.75$ and 1.0, the angle β for the forebody vortices decreases during the upstroke as the base moves downward and the angle of attack changes from $\alpha = 0$ to 30 deg. As the base moves upward during the downstroke and α changes from 30 to 0 deg, the angle β for the rearward vortices increases, reaching values as high as 135 deg.

The variation of β with x/L for the forebody vortex pair is shown in Fig. 11. Here, $\alpha = 15$ deg during the upstroke, the Reynolds number is $R_D = 4 \times 10^3$, and the reduced frequency is $K = 0.2$. At $x/L = 0.25$, $\beta = 25$ deg and increases to about 75 deg at the base of the body. In the present experiments, the angle β generally increased as the reduced frequency increased. At lower K, both vortex pairs are generally located near the top surface. However, at large reduced frequencies the oscillating motion of the body affects the vortices significantly and extreme values of β are achieved.

Reynolds Number Effects

The Reynolds number affects the geometry of the separation vortices over a missile moving at a constant angle of attack. The steady-state values for the vortex height H at different attack angles are plotted in Fig. 10 for two Reynolds numbers, $R_D = 4 \times 10^3$ and 4×10^4. Reynolds number effects are more pronounced at high angles of attack. At $\alpha = 30$ deg, the vortex height for the higher Reynolds number is about half that at the lower speed. At the low Reynolds number, the boundary layer in the attached flow region was transitional and intermittent regions of turbulence could be observed from the dye visualizations. At a Reynolds number of $R_D = 4 \times 10^4$, the boundary-layer flow was turbulent and the dye marking the separation vortices was observed to be well mixed.

For the unsteady case, Reynolds number effects are not as pronounced. Figure 12 shows the vortex height variation with angle of attack for the aftbody vortex pair at two Reynolds numbers, $R_D = 8 \times 10^3$ and 4×10^4. The reduced frequency for both runs is $K = 0.04$ and H is measured at $x/L = 0.75$. At this relatively** low reduced frequency, the flow appears to be similar to the steady-flow case, although a hysteresis loop still exists. During the downstroke, the height of the aftbody vortex pair is reduced by about 25% as the Reynolds number is increased by a factor of five. On the other hand, the forebody vortex pair stays near the top of the body and the angle β does not vary significantly with the angle of attack.

At higher reduced frequencies, the unsteady effects dominate the flow and are mainly responsible for the variations of the aerodynamic properties. Existing studies on two-dimensional, unsteady airfoils have shown that the Reynolds number is not a primary control parameter.[8] (However, see Refs. 44 and 45 for review of scaling problems in dynamic tests.) Also, as shown by the experiments reported in Refs. 46 and 47, while viscous effects are essential for producing the shear layer responsible for the onset of unsteady separation, viscosity does not play an important role on the subsequent dynamical processes within the already separated flow. In the present investigation, at a reduced frequency of $K = 0.2$, there was no measurable difference in the values of H when the Reynolds number is increased over one order of magnitude. In fact, the reduced frequency becomes the primary control parameter as the moving-wall effects dominate.[25,26] As shown in Figs. 10 and 12, the hysteresis loop is quite different when the reduced frequency changes from $K = 0.04$ (Fig. 12) to $K = 0.2$ (Fig. 10).

**The value $K = 0.04$ is rather large as far as moving-wall effects are concerned.[43]

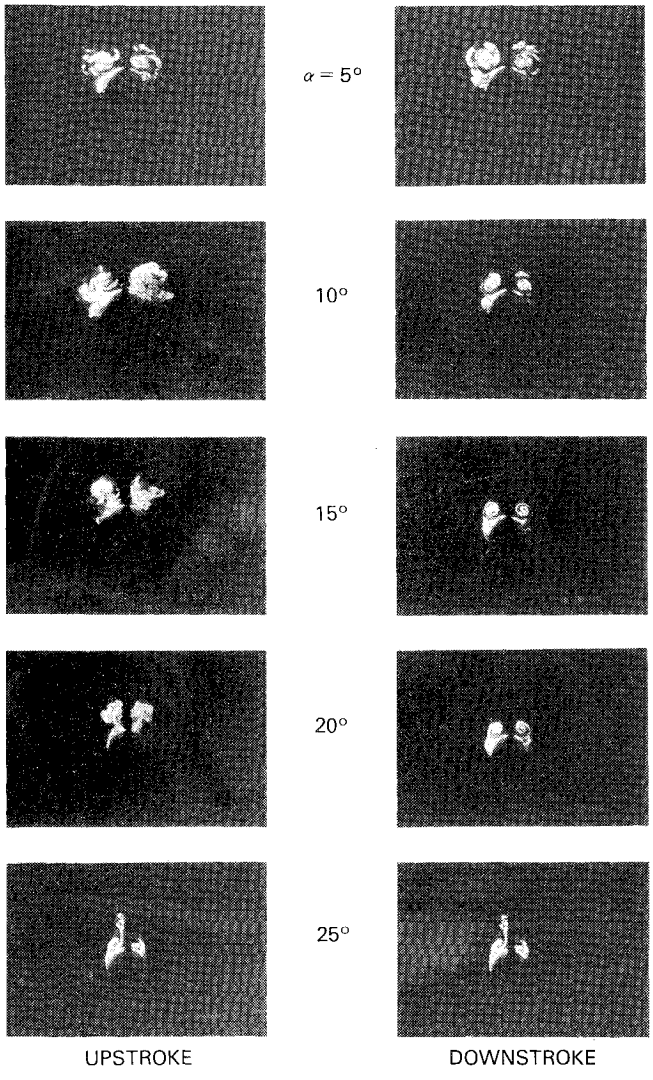

Fig. 13 Effects of oscillation amplitude: $R_D = 4 \times 10^3$; $K = 0.2$; $\alpha(t)^\circ = 15 + 10^\circ \sin(t)$ (sheet of laser is perpendicular to the flow at $x/L = 0.75$).

Pitching Parameters Effects

Adler and Luttges[16] have concluded that subtle changes in pitching parameters induce significant effects in the resulting flowfield around a three-dimensional rectangular wing. To investigate these effects for the pitching slender body, the sinusoidal oscillation amplitude was varied in the range of 5-15 deg about a given mean angle of attack. Figure 13 shows an end view of the slender body undergoing the pitching motion $\alpha(t)$ deg $= 15 + 10$ deg $\sin(t)$. The Reynolds number based on the diameter was $R_D = 4 \times 10^3$, and the reduced frequency was $K = 0.2$. Dye seeped continuously from the porous body surface and was excited using a vertical sheet of laser light perpendicular to the flow and located at $x/L = 0.75$. The photographs in Fig. 13 show a typical oscillation cycle for both the upward and downward motions of the body at $\alpha = 5$, 10, 15, 20, and 25 deg. The reduced frequency, Reynolds number, mean angle of attack, and visualization station for the run depicted in Fig. 13 are the same as those for the run shown in Fig. 7. Only the oscillation amplitude changed from ± 15 deg in Fig. 7 to $\pm$ 10 deg in Fig. 13. The effect on the leeward vortices is dramatic. Their size, circulation, and degree of symmetry change as the oscillation amplitude is reduced by 30%.

The angle β between the plane of symmetry of either the foreward or aft vortex pair and the vertical axis increased monotonically as the oscillation amplitude increased in the range of $\pm$5-15 deg. This could be explained by considering the shear generated by the harmonic motion of the body. Larger amplitude oscillation results in a thinner separation shear layer and more concentrated vorticity. The vortex roll-up is then more pronounced and β is larger.

IV. Conclusions

The complex flow patterns on a pitching slender body were visualized by using fluorescent dye techniques. The slender body was an ogive cylinder that was towed in an 18 m water channel and was undergoing a large-amplitude, harmonic pitching motion about the midbody at $x/L = 0.5$. It was found that the unsteady separation phenomenon was significantly different from the separation around the body in steady flight. Two separation vortex pairs were identified as the slender body underwent a complete pitching cycle. In this paper, these pairs were termed "forebody and aftbody separation vortices." During the upstroke, the unsteady separation starts near the base of the body and propagates upstream as the angle of attack increases. During the downstroke, the separated zone moves downstream and a secondary separation seems to be triggered by the primary separation near the nose of the body. Both separation regions are in the form of counter-rotating vortex pairs that undergo a growth/decay cycle.

The size, circulation, and degree of symmetry of the leeward vortices change dramatically with changes in the pitching parameters. On the other hand, at moderate-to-large reduced frequencies, the Reynolds number effects are negligible. The unsteady effects dominate the viscous effects and are mainly responsible for the variations of the aerodynamic properties.

The present investigation provides a closer look at the unsteady motion around a body of revolution undergoing a pitching motion. Other modes of unsteadiness should also be studied, such as plunging or time-dependent ambient velocity. References 6 and 18 indicate that the mode of the unsteady motion can significantly affect the hystersis loops and the aerodynamic properties of a lifting surface.[12] The results of the visualization experiments should be used to design fast-response probe experiments to measure the velocity field and to correlate the visualization events with the unsteady forces and moments experienced by the slender body.

Acknowledgments

This work is supported by the U.S. Air Force Office of Scientific Research, under Contract F49620-85-C-0028 and monitored by Dr. J. D. Wilson. The authors would like to acknowledge the valuable help of Messrs. M. Cooper, C. Shih, and R. Srnsky.

References

[1]Herbst, W. B., "Dynamics of Air Combat," *Journal of Aircraft*, Vol. 20, July 1983, pp. 594-598.

[2]Herbst, W. B., "Supermaneuverability," *Unsteady Separated Flows*, edited by M. S. Francis and M. W. Luttges, University of Colorado Press, Boulder, 1983, pp. 1-9.

[3]Nielsen, J. N., "Missile Aerodynamics—Past, Present, Future," AIAA Paper 79-1819, Aug. 1979.

[4]McCroskey, W. J., Carr, L. W., and McAlister, K. W., "Dynamic Stall Experiments on Oscillating Airfoils," *AIAA Journal*, Vol. 14, Jan. 1976, pp. 57-63.

[5]Nayfeh, A. H., Mook, D. T., and Yen, A., "The Aerodynamics of Small Harmonic Oscillations Around Large Angles of Attack," AIAA Paper 79-1520, July 1979.

[6]Carta, F. O., "A Comparison of the Pitching and Plunging Response of an Oscillating Airfoil," NASA CR-3172, Oct. 1979.

[7]Konstadinopoulos, P., Mook, D. T., and Nayfeh, A. H., "A Numerical Method for General Unsteady Aerodynamics," AIAA Paper 81-1877, Aug. 1981.

[8]McCroskey, W. J., "Unsteady Airfoils," *Annual Review of Fluid Mechanics*, Vol. 14, Jan. 1982, pp. 285-311.

[9]McCroskey, W. J. and Pucci, S. L., "Viscous-Inviscid Interaction on Oscillating Airfoils in Subsonic Flow," *AIAA Journal*, Vol. 20, Feb. 1982, pp. 167-174.

[10]Robinson, M. C. and Luttges, M. W., "Unsteady Flow Separation and Attachment Induced by Pitching Airfoils," AIAA Paper 83-0131, Jan. 1983.

[11]Konstadinopoulos, P., Mook, D. T., and Nayfeh, A. H., "Numerical Simulation of the Subsonic Wing-Rock Phenomenon," AIAA Paper 83-2115, Aug. 1983.

[12]Ericsson, L. E. and Reding, J. P., "The Difference Between the Effects of Pitch and Plunge on Dynamic Stall," Paper 8 presented at Ninth European Rotorcraft Forum, Stresa, Italy, Sept. 1983.

[13]Ericsson, L. E. and Reding, J. P., "Unsteady Flow Modules for Dynamic Stall Analysis," *Journal of Aircraft,* Vol. 21, Aug. 1984, pp. 601-606.

[14]Walker, J. M. and Helin, H. E., "An Experimental Investigation of an Airfoil Undergoing Large Amplitude Pitching Motions," AIAA Paper 85-0039, Jan. 1985.

[15]Helin, H. E. and Walker, J. M., "Interrelated Effects of Pitch Rate and Pivot on Airfoil Dynamic Stall," AIAA Paper 85-0130, Jan. 1985.

[16]Adler, J. N. and Luttges, M. W., "Three-Dimensionality in Unsteady Flow about a Wing," AIAA Paper 85-0132, Jan. 1985.

[17]Ericsson, L. E., "Is Any Free Flight/Wind Tunnel Equivalence Concept Valid for Unsteady Viscous Flow?," *Journal of Aircraft,* Vol. 22, Oct. 1985, pp. 915-919.

[18]Chen, S.-H. and Ho, C.-M., "Unsteady Aerodynamics of a Plunging Airfoil," *Bulletin of the American Physical Society,* Vol. 30, Nov. 1985, p. 1701.

[19]Gad-el-Hak, M. and Ho, C.-M., "The Pitching Delta Wing," *AIAA Journal,* Vol. 23, Nov. 1985, pp. 1660-1665.

[20]Gad-el-Hak, M. and Ho, C.-M., "Unsteady Vortical Flow Around Three-Dimensional Lifting Surfaces," *AIAA Journal,* Vol. 24, May 1986.

[21]Szebehely, V. G. and Niederer, O. C., "Unsteady and Amplitude Effects on the Moment Derivatives of a Prolate Spheroid," David Taylor Model Basin, Bethesda, MD, Rept. 828, 1953.

[22]Sevik, M., "The Lift on an Oscillating Body of Revolution," Ph.D. Thesis, Pennsylvania State University, University Park, 1963.

[23]Smith, L. H., "Aerodynamic Characteristics of an Axisymmetric Body Undergoing a Uniform Pitching Motion," Ph.D. Thesis, Naval Postgraduate School, Monterey, CA, Dec. 1974.

[24]Smith, L. H. and Nunn, R. H., "Aerodynamic Characteristics of an Axisymmetric Body Undergoing a Uniform Pitching Motion," *Journal of Spacecraft,* Vol. 13, Jan. 1976, pp. 8-14.

[25]Ericsson, L. E. and Reding, J. P., "Steady and Unsteady Vortex-Induced Asymmetric Loads on Slender Vehicles," *Journal of Spacecraft and Rockets,* Vol. 18, March-April 1981, pp. 97-109.

[26]Ericsson, L. E. and Reding, J. P., "Dynamics of Forebody Flow Separation and Associated Vortices," *Journal of Aircraft,* Vol. 22, April 1985, pp. 329-335.

[27]Mendenhall, M. R., Perkins, S. C. Jr., and Lesieutre, D. J., "Prediction of the Nonlinear Aerodynamic Characteristics of Maneuvering Missiles," AIAA Paper 85-1776, Aug. 1985.

[28]Gad-el-Hak, M., Blackwelder, R. F., and Riley, J. J., "On the Growth of Turbulent Regions in Laminar Boundary Layers," *Journal of Fluid Mechanics,* Vol. 110, Sept. 1981, pp. 73-95.

[29]Gad-el-Hak, M., "The Use of the Dye-Layer Technique for Unsteady Flow Visualization," *Transactions of ASME, Journal of Fluids Engineering,* Vol. 108, March 1986, pp. 34-38.

[30]Nielsen, J. J., "Nonlinearities in Missile Aerodynamics," AIAA Paper 78-0020, Jan. 1978.

[31]Gad-el-Hak, M. and Blackwelder, R. F., "The Discrete Vortices from a Delta Wing," *AIAA Journal,* Vol. 23, June 1985, pp. 961-962.

[32]Cooper, M., Gapcynski, J. P., and Hasel, L. E., "A Pressure Distribution Investigation of a Fineness-Ratio-12.2 Parabolic Body of Revolution (NACA RM-10) at $M=1.59$ and Angles of Attack to 36°," NACA RM L52G14a, Oct. 1952.

[33]Ericsson, L. E. and Reding, J. P., "Review of Vortex-Induced Asymmetric Loads—Part I," *Zeitschrift fuer Flugwissenschaften Weltraumforsch.,* Vol. 5, March 1981, pp. 162-174.

[34]Ericsson, L. E. and Reding, J. P., "Review of Vortex-Induced Asymmetric Loads—Part II," *Zeitschrift fuer Flugwissenschaften Weltraumforsch.,* Vol. 5, June 1981, pp. 349-366.

[35]Carta, F. O., "Unsteady Normal Forces on an Airfoil in a Periodically Stalled Inlet Flow," *Journal of Aircraft,* Vol. 4, Sept.-Oct. 1967, pp. 416-421.

[36]Ericsson, L. E., "Comment on Unsteady Airfoil Stall," *Journal of Aircraft,* Vol. 4, Sept.-Oct. 1967, pp. 478-480.

[37]Ericsson, L. E. and Reding, J. P., "Unsteady Airfoil Stall, Review and Extension," *Journal of Aircraft,* Vol. 8, Aug. 1971, pp. 609-616.

[38]McAlister, K. W. and Carr, L. W., "Water Tunnel Visualizations of Dynamic Stall," *Nonsteady Fluid Dynamics,* edited D. E. Crow and J. A. Miller, ASME, New York, 1978, pp. 103-110.

[39]McCroskey, W. J., McAlister, K. W., Carr, L. W., Pucci, S. L., Lambert, O., and Indergrand, R. F., "Dynamic Stall on Advanced Airfoil Sections," *Journal of the American Helicopter Society,* Vol. 13, July 1981, pp. 40-50.

[40]Ericsson, L. E. and Reding, J. P., "Re-entry Capsule Dynamics," *Journal of Spacecraft and Rockets,* Vol. 8, June 1971, pp. 575-586.

[41]Reding, J. P. and Ericsson, L. E., "Dynamic Support Interference," *Journal of Spacecraft and Rockets,* Vol. 9, July 1972, pp. 547-553.

[42]Gad-el-Hak, M., Blackwelder, R. F., and Riley, J. J., "Visualization Techniques for Studying Transitional and Turbulent Flows," *Flow Visualization,* Vol. 3, edited W. J. Yang, Hemisphere Publishing Corp., New York, 1983, pp. 568-575.

[43]Ericsson, L. E., "Karman Vortex Shedding and the Effect of Body Motion," *AIAA Journal,* Vol. 18, Aug. 1980, pp. 935-944.

[44]Ericsson, L. E. and Reding, J. P., "Reynolds Number Criticality in Dynamic Tests," AIAA Paper 78-166, Jan. 1978.

[45]Ericsson, L. E. and Reding, J. P., "Scaling Problems in Dynamic Tests of Aircraft-Like Configurations," AGARD-CP-227, Feb. 1978, Paper 25.

[46]Nishioka, M., Asai, M. and Iida, S., "An Experimental Investigation of the Secondary Instability," *Laminar-Turbulent Transition,* edited by R. Eppler and H. Fasel, Springer-Verlag, New York, 1980, pp. 37-46.

[47]Didden, N. and Ho, C.-M., "Unsteady Separation in a Boundary Layer Produced by an Impinging Jet," *Journal of Fluid Mechanics,* Vol. 160, Nov. 1985, pp. 235-256.